The Astrophysical Journal, 865:66 (5pp), 2018 September 20 https://doi.org/10.3847/1538-4357/aad9a2
© 2018. The American Astronomical Society. All rights reserved.

Depletion of FeO in the Interstellar Medium via Its Anion Resonances

Roby Chacko[1], Shreyak Banhatti[1], R. G. Mane[2], A. K. Gupta[2], and G. Aravind[1]
[1] Indian Institute of Technology Madras, Chennai 600 036, India; garavind@iitm.ac.in
[2] Nuclear Physics Division, Bhabha Atomic Research Centre, Mumbai 400 085, India
Received 2018 April 20; revised 2018 July 13; accepted 2018 August 8; published 2018 September 21

Abstract

Depletion of FeO in the interstellar medium through resonance states of FeO^- was studied through collision-induced dissociation of FeO^-. Collisional excitation of FeO^- lead to the yield of Fe^- and O^-, with a higher yield for Fe^-. The ground electronic state of FeO^- was identified to be $^6\Delta$ state and the results are compared with previous theoretical and experimental results. The kinetic energy distributions of the fragments revealed two FeO^- anion resonances accessed upon excitation and their potential energy curves were evaluated. The role of the observed resonances in the depletion of FeO and the viable presence of Fe^- and O^- in Sagittarius B2 are discussed.

Key words: astrochemistry – methods: laboratory: molecular – molecular processes – techniques: spectroscopic

1. Introduction

Anions have only recently been detected in the interstellar medium (ISM) although their presence was predicted more than three decades earlier (Herbst 1981). All six anions observed in the ISM are carbon containing species such as C_6H^- (McCarthy et al. 2006; Sakai et al. 2007), C_4H^- (Cernicharo et al. 2007; Gupta et al. 2007), C_8H^- (Gupta et al. 2007; Kawaguchi et al. 2007; Remijan et al. 2007), and C_nN^-(n = 1, 3, 5) (Thaddeus et al. 2008; Vuitton et al. 2009; Agúndez et al. 2010). Anions outside the carbon family are yet to be detected in the ISM. Metal oxides such as FeO, TiO, SiO, VO, CrO, YO, and ZrO were observed in the stellar atmosphere; however, their anionic states are yet to be observed in these environments. Furthermore, the depletion of refractory elements in the ISM influences the failure of their detection in the ISM. However, iron-bearing molecules such as FeO (Merer et al. 1982; Furuya et al. 2003) and FeCN (Zack et al. 2011) were detected in Sagittarius B2 and IRC+10216, respectively. Identification of the anionic states of ISM molecules such as FeO requires knowledge of the electronic and rovibrational states of the anion. Diatomic transition-metal anions such as TaC^-(Aravind et al. 2015) and WC^- (Sickafoose et al. 2002) have been observed to possess excited anionic states that are stable against autodetachment, a feature uncommon for diatomic anions. Rotational and vibrational transitions pertaining to such stable-excited states of anions need to be compared with the diffused interstellar bands to establish their presence in the ISM. Furthermore, anion resonances, which are excited electronic states embedded in the detachment continuum, determine the formation of smaller anions and neutrals upon resonant electron attachment to ISM molecules. Excitation to different resonances would lead to different fragmentation channels. Most importantly, astrophysical models that evaluate the abundance of both anions and their neutral state need to consider these resonance states. Theoretical studies of anion resonances are formidable and limited due to electron correlations and they are vastly probed through dissociative electron attachment (DEA) experiments (Ómarsson et al. 2014). The identification of ISM anions has been limited by the lack of sufficient spectroscopic and theoretical studies that consider astrophysical environments (Forternburry 2015).

In the present work, we probe resonance states of the FeO^- anion whose neutral state is already identified in Sagittarius B2. Since FeO in the ISM can undergo DEA through these resonances, the present work on FeO^- resonances is of paramount importance for evaluating the abundance and stability of FeO in Sagittarius B2. Theoretical studies on resonances in FeO^- have, to the best of our knowledge, not been performed while autodetachment spectroscopy on FeO^- has been performed by Andersen et al. (1987). Autodetachment spectroscopy revealed rich resonances, both valence and dipole-bound states of the anion. The electronic states of FeO are highly congested and a similar feature is expected of the FeO^- states rendering the autodetachment spectra complex. The electronic state of FeO^- had been studied through photoelectron spectroscopy (Engelking & Lineberger 1977; Fan & Wang 1995; Kim et al. 2015), identifying various stable electronic states of the anion. Theoretical calculations (Hendrickx & Anam 2009; Sakellaris et al. 2011) identify $^6\Sigma^+$ as the ground electronic state of FeO^- while experiment (Kim et al. 2015) infers it to be $^4\Delta$. Gutsev et al. (1999) have studied the electronic and geometrical structures of the ground and a few excited states of FeO_n^- (n = 1–4).

We probe the resonances in FeO^- through collisional excitation of FeO^- and study their evolution and its relevance to ISM. Gas phase DEA studies on FeO is challenging, leaving collision-induced dissociation (CID), the technique of the present work, and photoexcitation of FeO^- as the most viable means to probe these resonances. The resonance states also determine the reactions involving atomic iron and iron-bearing molecules in the ISM. The present results on FeO^- resonances are important in understanding the stability of FeO in Sgr B2 and in modeling their abundance.

2. Experimental Section

The experimental setup employed in this work is described in detailed elsewhere (Gupta & Krishnamurthy 2003). FeO^- anions were produced by sputtering 1 keV Cs ions on Fe_2O_3 pellets. The anions thus produced were accelerated to 15 keV and a double focusing 90° magnet was used to mass separate the ions of interest. The mass selected ions were allowed to collide with Argon in the collision cell. The chamber pressure

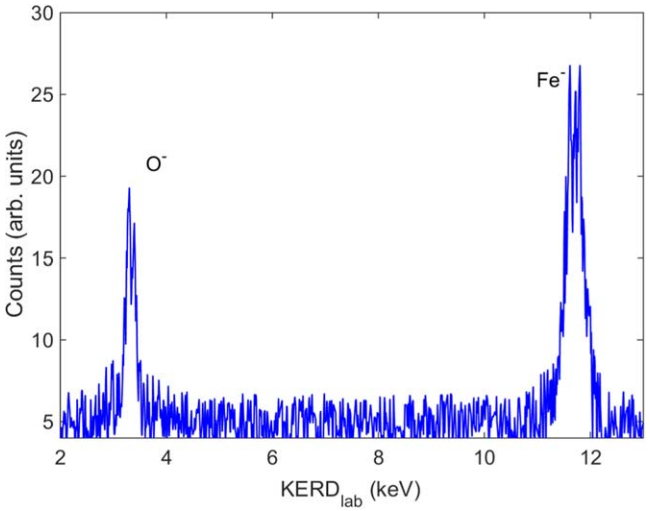

Figure 1. Lab-frame kinetic energy distribution ($KERD_{lab}$) of Fe^- and O^- fragments from CID of FeO^-.

was 3×10^{-6} Torr with a base pressure of about 1×10^{-7} Torr. Only those ions scattered in the forward and backward directions (angular resolution $\pm 0.01°$) were energy analyzed using a parallel-plate analyzer. Channeltron and pulse-counting electronics were used to detect the fragment ions. The energy analysis yields kinetic energy released in the lab frame.

3. Results and Discussion

3.1. Dissociation Dynamics of FeO^- Anion

FeO^- accelerated to 15 keV were collided with argon target gas resulting in their electronic excitation eventually leading to fragments. The electron affinity of FeO^- is 1.495 eV (Kim et al. 2015) while the dissociation energy is 3.31 eV (present work and Sakellaris et al. 2011) rendering even the higher vibrational states of the ground electronic state as autodetaching states. Hence there is no possibility for a purely repulsive excited state, lying even partially below the detachment continuum, accessed to yield the observed fragments. Although excited states of FeO^- have been identified, their geometries being similar to the ground state (Sakellaris et al. 2011), any Franck–Condon transition to the repulsive part of such excited states leading to the observed fragments is ruled out. Hence the excited states accessed in the collisional excitation leading to the observed fragment ions are anion resonances, which are embedded in the detachment continuum. Anion resonances decay via autodetachment or eventually dissociate yielding anionic and neutral fragments. The kinetic energy released during fragmentation is shared between the fragments in their inverse-mass ratio. Interestingly, we observed both Fe^- and O^- anion fragments in our experiment as in the case of FeC^- (Nrisimhamurty et al. 2016). Figure 1 shows the lab-frame kinetic energy distribution of both the anion fragments. We employ translational energy spectroscopy wherein the energy released in the Center-of-Mass (C.M. frame) gets amplified in the lab-frame energy distribution, enabling measurement of small energy release. Measurement of fragments scattered in the forward and backward direction in the C.M. frame eliminates events in which the target atoms are excited during collision. Furthermore, large impact collision results in electronic excitation rather than vibrational. The instrumental and initial spread in parent ion energy accounts for the width of

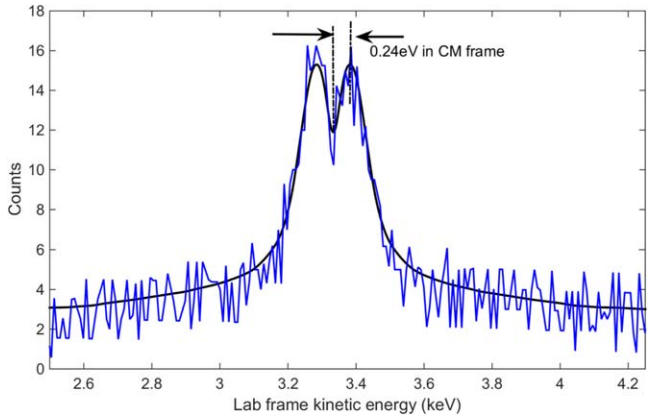

Figure 2. Lab-frame kinetic energy distribution ($KERD_{lab}$) of O^- fragments from CID of FeO^-. The energy separation indicated is in the C.M. frame energy scale.

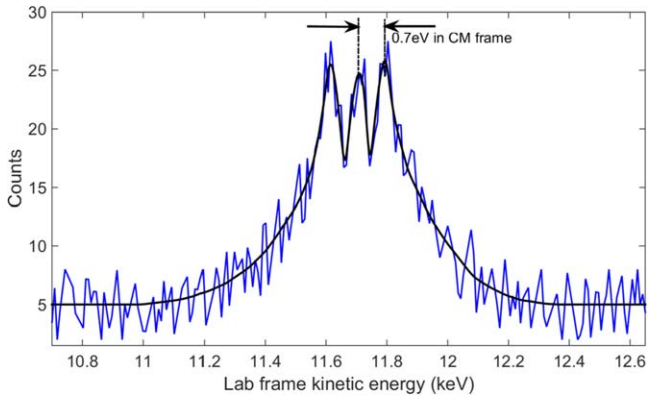

Figure 3. Lab-frame kinetic energy distribution ($KERD_{lab}$) of Fe^- fragments from CID of FeO^-. The energy separation indicated is in the C.M. frame energy scale.

the lab-frame kinetic energy of the parent. The kinetic energy distribution in the lab frame ($KERD_{lab}$) for the daughter ions was obtained by deconvoluting the measured lab-frame kinetic energy distribution with that of their parent. If E_1 is the lab-frame kinetic energy of a fragment ion m_1, then the total kinetic energy released in the C.M. frame, E_{CM}, is given by

$$E_1 = \frac{m_1}{M}E'_p + \frac{2\sqrt{E_{CM}E'_p m_1 m_2}}{M} + \frac{m_2}{M}E_{CM} \quad (1)$$

$$E'_p = (E_p - E_{CM} - Q), \quad (2)$$

where M and m_2 are masses of the parent ion and the neutral fragment, respectively, and Q is the total internal excitation energy for both the projectile and the target.

3.2. Determination of Kinetic Energy Release in the C.M. Frame and the Anion Resonances

Figures 2 and 3 show the lab-frame kinetic energy distribution for O^- and Fe^- anions, respectively. The distributions are a result of both the forward and backward ejection of fragments along the line of motion of the parent anions and hence the fragment velocity in the C.M. frame is added (forward) or subtracted (backward) to the lab-frame velocity of the parent anion.

Figure 4 explains the reflection of the initial state vibrational wavefunction upon the excited state resulting in the $KERD_{CM}$.

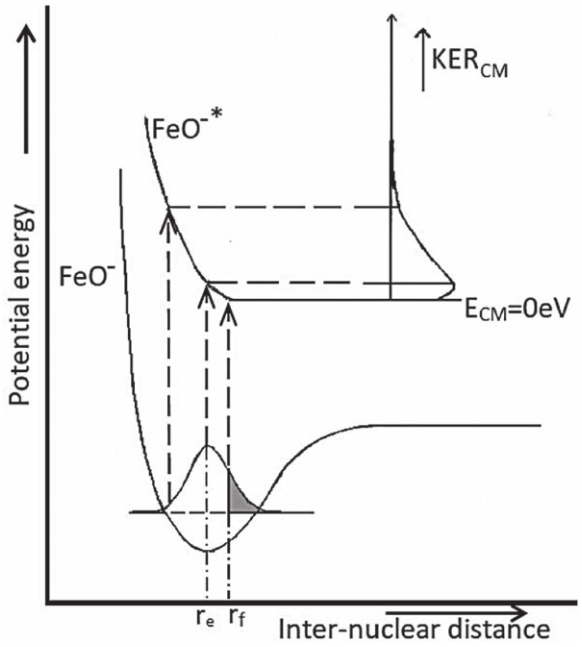

Figure 4. Schematic diagram describing kinetic energy release in the center-of-mass frame upon collisional excitation of the ground anion state to anion resonance.

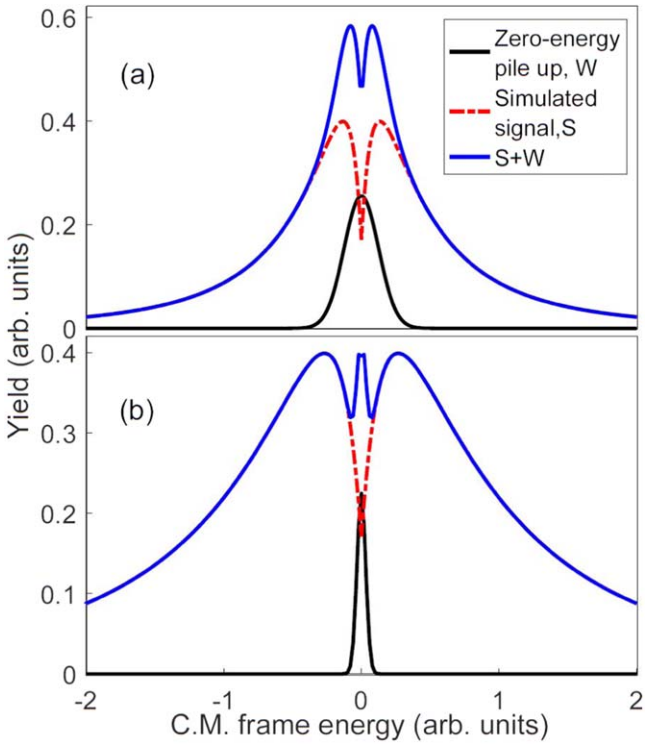

Figure 5. Simulation of double-peak (a) and multipeak structures (b) in the C. M. frame energy distribution. The positive and negative energies correspond to forward and backward scattering of the ions, respectively.

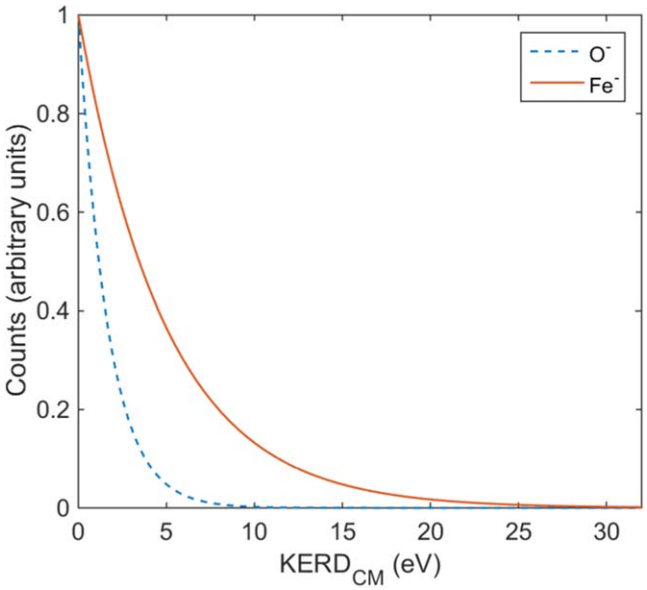

Figure 6. Center-of-Mass frame kinetic energy distribution (KERD$_{CM}$) of Fe^- and O^- fragments from CID of FeO^-.

r_e is the internuclear distance at which the ground electronic state's vibrational wavefunction reaches its maximum value. r_f is the internuclear distance at which the repulsive curve reaches its asymptotic value. $KERD_{CM}$ depends on the shape of the anion resonance curve accessed by the parent ion before dissociation as well the initial state vibrational wavefunction. If $r_e < r_f$, as shown in the figure, then $E_{CM} = 0$ for all the anions excited with initial bond length greater that r_f (as in the shaded region of the figure). This will result in a pile up at $E_{CM} = 0$ for $KERD_{CM}$. The vector addition of forward and backward C.M. frame momenta to the lab-frame momentum results in two-peak structure in the lab frame and in addition, the pile up at $E_{CM} = 0$, broadened by instrumental resolution, yields a three-peak structure. It is this three-peak structure that is depicted in Figure 5(b) and explains the observed peak in Figure 3. If the central peak is less intense, which is the case when r_f is too close to the turning point in the ground electronic state, or if the two peaks stemming from the forward and backward momenta additions are too close, then the central peak may not be manifested in the experimental data. This is depicted in Figure 5(a) and explains the observed peak in Figure 2. If $r_f \leqslant r_e$, only a single peak is expected in $KERD_{CM}$. If r_f is greater than r_e, but is very close to r_e, the multiple peak structure may become unresolved due to limitations in the resolution of the energy analyzer. In Figures 2 and 3, though the multiple peak structures are evident, they are not well-resolved to perform numerical deconvolution with the given instrumental width as the peaks lie very close to $E_{CM} = 0$. The close proximity of r_f and r_e in the present case justifies approximation of the $KERD_{lab}$ to a Gaussian profile. Hence a Gaussian profile was employed for $KERD_{lab}$ to perform the deconvolution. The deconvoluted $KERD_{lab}$ was then used to obtain $KERD_{CM}$ using Equation (1).

The $KERD_{CM}$ thus obtained are shown in Figure 6. The $KERD_{CM}$ for Fe^- and O^- anion fragments are markedly different from each other. As the $KERD_{CM}$ is critically determined by the Franck–Condon overlap between the initial and final states and the shape of the resonance curve, the results clearly reveal excitation to two different anion resonances upon collisional excitation, each resulting in different anion fragments. In spite of lower electron affinity, the yield of Fe^- was found to be higher than that for O^- and a similar feature was observed earlier for FeC^- (Nrisimhamurty et al. 2016). To evaluate the potential energy curves of the resonances, we computed the ground electronic state of FeO^-.

Table 1
Comparison of the Present and Previous Results for Bond Length (r_e), and Bond-dissociation Energy (D_e) of the Ground State of FeO^-

Methodology	State	r_e (Å)	D_e (kcal mol^{-1})	ω_e (cm^{-1})
CCSD[a] (Level)	$^6\Delta$	1.75	76.3765	785.73
CASPT2[b]	$^6\Sigma^+$	1.683	⋯	807
MRCI—L + DKH2+Q[c]	$^6\Sigma^+$	1.709	92.4	752
RCCSD(T) + DKH2[c]	$^6\Sigma^+$	1.690	93.9	857
C—RCCSD(T) + DKH2[c]	$^6\Sigma^+$	1.685	91.9	878
Experiment[d]	$^4\Delta$	1.647	⋯	740 ± 20

Notes.
[a] Present Results.
[b] Hendrickx & Anam (2009).
[c] Sakellaris et al. (2011).
[d] Drechsler et al. (1997).

The ground electronic state of FeO^- was calculated using the coupled cluster method (CCSD level) using the TZV basis set. Table 1 compares the present results with the previous theoretical and experimental results. Our calculation identifies $^6\Delta$ as the ground state. Photoelectron and autodetachment spectroscopic studies (Andersen et al. 1987; Kim et al. 2015) indicate $^4\Delta$ as the ground electronic state. The vibrational wavefunctions, which determine the anion resonance, are expected to be similar for $^6\Delta$ and $^4\Delta$ as they are nearly degenerate over a wide range of internuclear distances and also have similar bond lengths. Figure 7 shows the calculated ground state potential energy curve. The vibrational state wavefunctions for this ground electronic state were calculated using LEVEL (Le Roy 2015). This program computes rovibrational eigenvalues and eigenfunctions for smoothly varying one-dimensional or radial potential energy functions using the semi-classical WKB method. Under the temperature condition of the ion-source, the first four vibrational levels of the ground electronic state of FeO^- would have significant populations. Vibrational wavefunctions of these levels were statistically weighed and the inset in Figure 7 shows the probability density of the resultant wavefunction. Reflection of this probability distribution on the potential energy curve of the resonance yields the C.M. frame kinetic energy release distribution. The potential energy curve of the resonance is hence deduced from the kinetic energy release distribution. The section of the anion resonance curve that can be spanned by our experiment is determined by the Franck–Condon overlap. By assuming a delta-function at the classical turning point as the wavefunction at the excited resonance the anion resonances were evaluated as shown in Figure 8. The asymptotic limit for the resonance dissociating into O^- is Fe(^{5}D) + O^-(^{2}P) and that of the resonance leading to Fe^- is Fe^-(^{4}F) + O(^{3}P). The energy spacing between the asymptotes of the two evaluated resonances is determined by the binding energies of the fragment anions (Engelking & Lineberger 1979; Blondel et al. 2005). Our results show the anion resonance curve for the range of internuclear distance spanned in our experiment. The dotted part of the resonance curves do not pertain to the region spanned by our experiment and this region could have a shallow well or simply tend to the dissociation limit if the resonance is purely repulsive. Although autodetachment spectroscopy can identify the resonances, the present result evaluates the resonance potential energy curves, most importantly the fragmentation pathways for FeO.

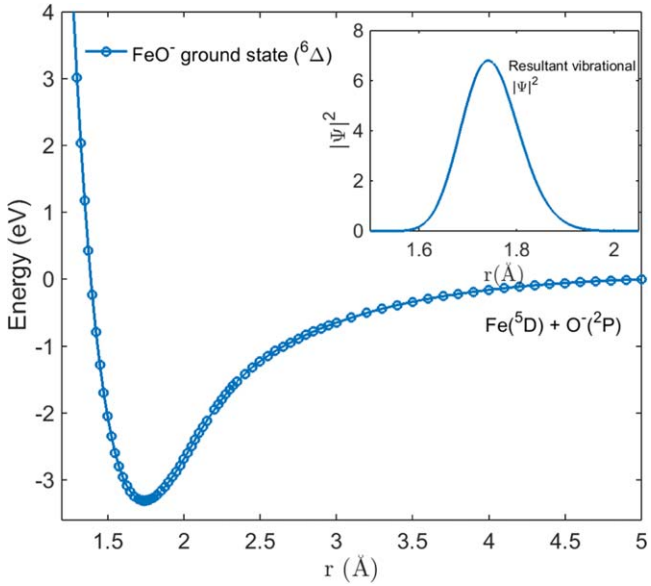

Figure 7. Ground electronic state of FeO^- was calculated to be $^6\Delta$ using the coupled cluster method (CCSD level) using the TZV basis set. The inset shows the resultant vibrational probability density calculated using LEVEL (Le Roy 2015; see the text).

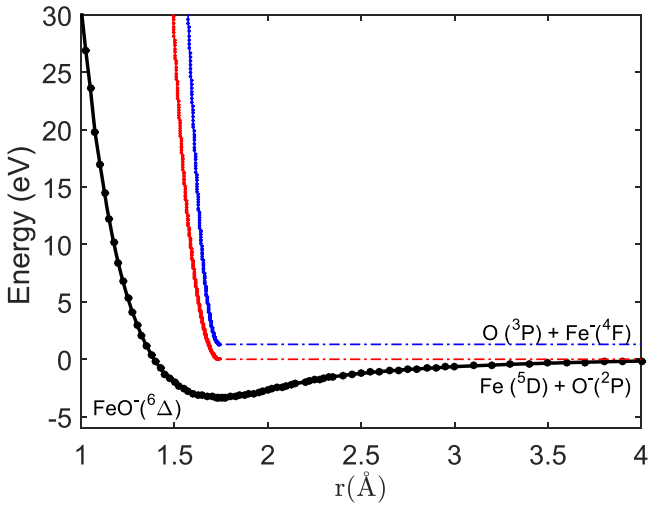

Figure 8. Potential energy curves for the two anion resonances accessed in the collisional excitation of FeO^-.

3.3. Astrophysical Relevance

FeO could be expelled from the grains during a shock in Sagittarius B2. It could also be formed endothermically but only under shocked gas conditions since high temperature is required to form FeO from Fe and O_2 (Walmsley et al. 2002). The electron affinity of FeO is 1.49 eV (Engelking & Lineberger 1977) and our results show the presence of FeO^- resonances 3.31 eV above the ground state of the anion. Thus a resonant electron attachment to FeO with an electron energy of about 1.81 eV should lead to the resonances observed in our experiment. Such a resonant electron attachment is feasible in the shocked gas conditions, particularly from higher vibrational states of FeO, leading to the decay of FeO into Fe^- or O^-. Our results show the dissociation pathways of FeO upon DEA in Sagittarius B2. In order for astrophysical models to evaluate the

abundance of FeO in the ISM, in addition to the processes forming the molecule, the mechanisms leading to its destruction need to be considered. Our results emphasize that DEA can play a dominant role as a depletion mechanism for this molecule in Sagittarius B2. Furthermore, the ratio of column densities for FeO and SiO ([FeO]/[SiO]) is known to be about 0.01 and the slower rate of the endothermic reaction leading to FeO is considered to be the reason for its lower density (Walmsley et al. 2002). The role of resonances in the depletion of FeO should also be considered in understanding the lower density of FeO. Anions of transition-metal carbides and oxides are known to possess dense electronic states that are stable against electron detachment and are expected to have many resonances close to their detachment continuum. Hence the depletion mechanism in FeO, through its anion resonance, is expected to be more dominant than in SiO explaining the observed ratio of their column densities. The observed resonances in FeO^- dominantly decay into Fe^-, which is consistent with the astronomical data that suggest the abundance of gas phase Fe than FeO in the ISM (Merer et al. 1982). Atomic oxygen has been detected in Sagittarius B2 by observing the 63 μm ground-state fine-structure line (Baluteau et al. 1997). Nearly 40% of oxygen in this molecular cloud is in the form of atomic oxygen. Formation of O^- and Fe^- from the resonance states of FeO^-, as observed in our experiment, suggest the search for these two atomic anions in the Sagittarius B2. In the case of O^- the emission line corresponding to ($^2P_{3/2}$–$^2P_{1/2}$) is 56.47 μm (Blondel et al. 2001). Emission line corresponding to 56.34 μm observed in Sgr B2 is close to this line and had been assigned to NH_3 (Ceccarelli et al. 2002). Fe^- has four fine-structure levels ($^4F_{9/2}$, $^4F_{7/2}$, $^4F_{6/2}$, and $^4F_{3/2}$). The emission line corresponding to the dipole-allowed transition ($^4F_{9/2}$–$^4F_{7/2}$) is 19.19 μm (Chen et al. 2016) and should be searched for in the region where FeO is detected. Furthermore, in the dense clouds, electron attachment to FeO leading to stable FeO^- states is possible.

4. Conclusions

The depletion of FeO in ISM via resonances of FeO^- was probed by collisional excitation of FeO^-. The kinetic energy released in the C.M. frame was employed to find two anion resonances that decay into Fe^- and O^-. The results show that upon resonant electron attachment to FeO in ISM it would predominantly decay into Fe^- than O^-. The potential energy curves for the two anion resonances, in the region spanned by our experiment, were evaluated. Although previous autodetachment spectroscopy on FeO^- identified anion resonances, to the best of our knowledge, the present result is the first to evaluate their potential energy curves and the eventual decay pathways. The ground electronic state of FeO^- was identified to be $^6\Delta$, in agreement with the previous theoretical results. The observed resonances in FeO^- and their binding energies relative to the ground electronic state indicate its dominant role in the depletion of FeO in Sagittarius B2. To the best of our knowledge, there are no DEA experiments performed on FeO. The present results emphasize the need to include the decay of FeO through FeO^- anion resonance in the astrophysical models that compute their abundance. Relative abundance of FeO and SiO and the influence of FeO^- resonances on it is also discussed. The present results motivate the search for O^- (56.34 μm) and Fe^-(19.19 μm) in Sagittarius B2. The present results on FeO^- resonances are of paramount importance in understanding the depletion of iron-bearing molecules in the ISM. We believe that the search for FeO^- will shed more light on the astrochemistry of iron-bearing molecules.

We acknowledge the assistance provided by Dr. Y. Sajeev in the present theoretical calculations. This project was funded by the Department of Science and Technology (DST), India, under the grant No. SR/S2/LOP-04/2012.

References

Agúndez, M., Cernicharo, J., Guélin, M., et al. 2010, A&A, 517, L2
Andersen, T., Lykke, K. R., Neumark, D. M., & Lineberger, W. C. 1987, JChPh, 86, 1858
Aravind, G., Nrisimhamurty, M., Mane, R. G., Gupta, A. K., & Krishnakumar, E. 2015, PhRvA, 92, 042503
Baluteau, J. P., Cox, P., Cernicharo, J., et al. 1997, A&A, 322, L33
Blondel, C., Chaibi, W., Delsart, C., et al. 2005, EPJD, 33, 335
Blondel, C., Delsart, C., Valli, C., et al. 2001, PhRvA, 64, 052504
Ceccarelli, C., Baluteau, J. P., Walmsley, M., et al. 2002, A&A, 383, 603
Cernicharo, J., Guélin, M., Agúndez, M., et al. 2007, A&A, 467, L37
Chen, X., Luo, Z., Li, J., & Ning, C. 2016, NatSR, 6, 24996
Drechsler, G., Boesl, U., Babmann, C., & Schlag, E. W. 1997, JChPh, 107, 2284
Engelking, P. C., & Lineberger, W. C. 1977, JChPh, 66, 5054
Engelking, P. C., & Lineberger, W. C. 1979, PhRvA, 19, 149
Fan, J., & Wang, L. 1995, JChPh, 102, 8714
Forternburry, RC. 2015, JPCA, 119, 9941
Furuya, R. S., Walmsley, C. M., Nakanishi, K., Schilke, P., & Bachiller, R. 2003, A&A, 409, L21
Gupta, A. K., & Krishnamurthy, M. 2003, PhRvA, 67, 023201
Gupta, H., Brünken, S., Tamassia, F., et al. 2007, ApJL, 655, L57
Gutsev, G. L., Khanna, S. N., Rao, B. K., & Jena, P. 1999, JPCA, 103, 5812
Hendrickx, F. A., & Anam, K. R. 2009, JPCA, 113, 8746
Herbst, E. 1981, Natur, 289, 656
Kawaguchi, K., Fujimori, R., Aimi, S., et al. 2007, PASJ, 59, L47
Kim, J. B., Weichman, M. L., & Neumark, D. M. 2015, MolPh, 113, 2105
Le Roy, R. J. 2015, LEVEL 8.2: A Computer program for solving the radial Schrödinger equation for bound and quasibound Levels, Chemical Physics Research Rep. CP-668 (Waterloo: Univ. Waterloo), http://scienide2.uwaterloo.ca/rleroy/level/
McCarthy, M. C., Gottlieb, C. A., Gupta, H., & Thaddeus, P. 2006, ApJL, 652, L141
Merer, A. J., Walmsley, C. M., & Churchwell, E. 1982, ApJ, 256, 151
Nrisimhamurty, M., Mane, R. G., Chacko, R., et al. 2016, ApJ, 833, 269
Ómarsson, F. H., Mason, N. J., Krishnakumar, E., & Ingólfsson, O. 2014, Angew. Chem. Int. ed., 53, 12051
Remijan, A. J., Hollis, J. M., Lovas, F. J., et al. 2007, ApJL, 664, L47
Sakai, N., Sakai, T., Osamura, Y., & Yamamoto, S. 2007, ApJL, 667, L65
Sakellaris, C. N., Miliordos, E., & Mavridis, A. 2011, JChPh, 134, 234308
Sickafoose, S. M., Smith, A. W., & Morse, M. D. 2002, JChPh, 116, 993
Thaddeus, P., Gottlieb, C. A., Gupta, H., et al. 2008, ApJ, 677, 1132
Vuitton, V., Lavvas, P., Yelle, R. V., et al. 2009, P&SS, 57, 1558
Walmsley, C. M., Bachiller, R., Pineau des Forêts, G., & Schilke, P. 2002, ApJL, 566, L109
Zack, L. N., Halfen, D. T., & Ziurys, L. M. 2011, ApJL, 733, L36